Micro-structured ZSM-11 catalyst on stainless-steel microfibers for improving glycerol dehydration to acrolein

Jia Ding,[†] Lizhuo Wang,[†] Zhiqiang Zhang,[‡] Shufang Zhao,[†] Yong Lu,[,‡] and Jun Huang[*,†]*

† Laboratory for Catalysis Engineering, School of Chemical and Biomolecular Engineering, Sydney Nano Institute, The University of Sydney, New South Wales 2006, Australia

‡ Shanghai Key Laboratory of Green Chemistry and Chemical Processes, School of Chemistry and Molecular Engineering, East China Normal University, Shanghai 200062, China.

ABSTRACT: Glycerol is a byproduct from the biodiesel manufacturing. Glycerol dehydration into more valuable acrolein is desirable and essential since it improves the economics of the biodiesel production and offers a sustainable route to replace the market favorite chemical from petroleum process. Zeolites with the dominant Brønsted acid sites have been wildly used in glycerol dehydration, since Brønsted acid sites are flexible and interacting with the center hydroxyl of glycerol towards acrolein production. In this research, microstructured ZSM-11 catalysts have been developed by direct growth of zeolite crystals on a macroscopic 3D network of sinter-locked stainless-steel microfibers. It showed remarkable stability and acrolein selectivity improvement as compared to conventional ZSM-11 zeolite, due to the short residence time to limit the secondary reactions and enhanced mass transfer to minimize the coke formation. The acidity of zeolites has been optimized via tuning the SiO_2/Al_2O_3 ratios in a wide range from 78 to 283. The highest glycerol conversions and acrolein selectivity were observed over the catalyst with a SiO_2/Al_2O_3 molar ratio of 131. The higher temperature at 300 ^oC was necessary to achieve better catalytic conversion and improve the acrolein formation. At the high-flow of carrier gas, the coke formation was suppressed due to the enhanced diffusion of big-size products out of the zeolite pores.

KEYWORDS: Microstructured catalyst; ZSM-11 zeolite; Dehydration of glycerol; Acrolein; Stability

1. INTRODUCTION

Biodiesel production has attracted intensive attentions worldwide because this sustainable fuel process uses renewable fats and vegetable oils to replace fossil fuels as raw materials [1]. In the last decade, the increase of biodiesel manufacturing has generated large quantities of glycerol as byproduct more than the market needs, which results in the environmental challenge to store it proportionally [2]. Hence, the transformation of glycerol into more valuable products is desirable and essential since it improves the economics of biodiesel production and, at the same time, provides important and versatile industrial feedstocks. Generally, glycerol can undergo dehydration, oxidation, reforming, hydrogenolysis, etherification and esterification reactions to produce a lot of chemical commodities [3-4]. Acrolein produced from dehydration of glycerol can be used for the production of acrylic acid, acid esters, super absorbers polymers, detergents, fragrances, dyes and agrochemicals like methionine, among other products. Currently, acrolein is carried out by partial oxidation of propylene from petroleum oil refining, using mixed metal oxides as catalysts [5-6]. Therefore, catalytic conversion of glycerol into acrolein offers a cost-effective and sustainable alternative route to replace the present production technology.

To date, various catalysts have been studied in the heterogeneous catalysis for dehydration of glycerol in the gas phase, such as metal oxides [7-12], metal phosphates [13], metal sulfates [14], acidic aluminosilicate [15], supported heteropolyacids [16] and acidic zeolites (MFI, BEA, FAU, MOR and MWW type) with different Si/Al ratios [17-23]. According to the reaction mechanism [24], the dehydration should be initiated by the central hydroxyl on acid sites and lead to 3-hydroxy-propanal, then followed by the further dehydration on the terminal hydroxyl to form acrolein. Parallelly, the dehydration initiated at terminal hydroxyl groups leads to the formation of acetol. It was reported that Brønsted acid sites are more flexible than Lewis acid sites and more easily to

access the central hydroxyl of glycerol for the dehydration to acrolein [25]. Meanwhile, Lewis acid sites are more accessible for terminal hydroxyl group to start dehydration and prefer to produce acetol. Hence, numerous efforts have been made to the dehydration of glycerol on zeolites, since the Brønsted acid sites are dominant with the uniform acidity in crystal zeolites via their framework Al species to form the bridging SiOHAl groups. The surface acidity of zeolites is depended on the Si/Al ratio of the framework, which can change the overall electronegativity of zeolites. Therefore, the most suitable SiO_2/Al_2O_3 molar ratio for glycerol dehydration toward acrolein was inconsistent for a different type of zeolites and still need to be investigated.

Moreover, the morphology and pore structures of zeolites can also be flexibly tuned toward better performance in glycerol dehydration [22, 26-31]. It is well-known that zeolites with different framework structures have their unique channel features, promoting or blocking for a certain reaction due to the shape-selectivity of zeolites for the reactants, intermediates, and products. ZSM-11 zeolite with MEL structure has slightly shifted straight channels with a diameter of 5.3 × 5.4 Å in two directions and 3-dimensionality at the interface between two perpendicular [32]. Gu et al. [23] reported that among the frequently-used zeolites, ZSM-11 showed higher stability and acrolein selectivity than Beta, Y and ZSM-5 for glycerol dehydration, due to its suitable channel diameter and helical channels with more ideal diffusion behavior.

Analogous to other consecutive reactions like methanol to olefins and n-hexane catalytic cracking [33-36], poor mass/heat transfer, high pressure drop, non-regular flow pattern, and adverse effects of the binders always reduced the intrinsic selectivity and activity of zeolite catalysts. To solve these problems, microstructured zeolite catalysts have been developed by mounting zeolites onto monolithic substrates, such as porous ceramic, silicon carbide and metal foam/fiber. For heterogeneous reactions, microstructured zeolite catalysts always showed dramatic

selectivity/stability improvement as compared to the unstructured counterparts [33-35]. Hence, developing microstructured zeolite catalysts is highly desirable and promising to achieve better performance for glycerol dehydration.

In this work, we demonstrate an in-situ growth of ZSM-11 layer on a thin-felt three-dimensional (3D) sinter-locked microfibrous support by the hydrothermal synthesis method. The obtained ZSM-11/SS-fiber catalysts were applied to glycerol dehydration reaction for the production of acrolein. The influences of the zeolite acidity by the various SiO_2/Al_2O_3 molar ratios, reaction temperatures, glycerol contents and carrier gas flow rates on catalytic performance were systematically investigated. Furthermore, the catalytic performance of ZSM-11/SS-fiber was compared to the ZSM-11 pellet to gain insight into the microstructured design.

2. EXPERIMENTAL SECTION

2.1. Catalyst preparation

2.1.1. Materials and chemicals

A thin-felt three-dimensional (3D) sinter-locked microfibrous structure consisting of 20 μm 316L SS-fiber (Western Metal Material Co. Ltd., China) was cut into circular chips (dia. 8 mm) and employed as the substrate. Prior to hydrothermal synthesis, the microfibrous-structured substrate was sonicated in acetone for 2 h, thoroughly washed by deionized water and then dried at 100 ^oC overnight. The following chemicals were used for the zeolite synthesis: tetraethylorthosilicate (TEOS, A.R., Sigma-Aldrich), colloidal silica (LUDOX® AS-30, Sigma-Aldrich), sodium aluminate ($NaAlO_2$, Tech., Sigma-Aldrich), tetrabutylammonium hydroxide (TBAOH, 25 wt.% in H_2O, Sigma-Aldrich), ammonium chloride (NH_4Cl, A.R., Sigma-Aldrich), and ammonium hydroxide (28~30 wt.% NH_3 in H_2O, Sigma-Aldrich). All reagents were used as received without further purification.

2.1.2. Preparation of silicalite-2 seeds

The nanosized silicalite-2 (pure silica and MEL-type zeolite) seeds were prepared from a clear solution with a molar ratio of TEOS: 0.35TBAOH: 15H_2O. The reaction solution was homogenized at room temperature for 24 h, and then sealed in a Teflon-lined stainless-steel autoclave and conducted at 90 ºC for 6 d. After cooling, the gel was centrifugated and washed by deionized water to obtain silicalite-2 seeds. After drying at 100 ºC for 24 h, silicalite-2 seeds were ground into powder.

2.1.3. Synthesis of ZSM-11/SS-fiber catalyst

The thin-felt ZSM-11/SS-fiber catalyst was synthesized by the hydrothermal method. Firstly, a certain amount of $NaAlO_2$, TBAOH and colloidal silica were dissolved in deionized water under stirring at room temperature to obtain a clear solution with a molar ratio of SiO_2: TBAOH: $NaAlO_2$: H_2O = 1: 0.2: (50~250): 250.

Thirty circular chips of SS-fiber substrate were seeded by silicalite-2 using the dip-coating method. The silicalite-2 seeds were dispersed in deionized water to obtain 2 wt.% suspension, which pH was adjusted to 10 using ammonium hydroxide. Then, SS-fiber substrate was dipped into the above suspension for 15 min with ultrasonic processing, followed by drying at 100 ºC for 12 h.

Subsequently, 70 mL of synthesis precursor and 30 circular chips of silicalite-2 seeded SS-fiber were sealed into a Teflon-lined stainless-steel autoclave and statically crystallized at 180 ºC for 48 h. The as-synthesized microfibrous-structured ZSM-11/SS-fiber composites were rinsed thoroughly with water, dried in oven at 100 ºC overnight, and calcined in air at 550 ºC for 5 h to remove the organic templates. Then, calcined ZSM-11/SS-fiber samples were converted into H-form by ion-exchange with an aqueous solution of 1 M ammonium chloride at 80 ºC for 3 h and

calcination at 550 ºC for 5 h. The obtained ZSM-11/SS-fiber catalysts with synthesis precursor SiO_2/Al_2O_3 molar ratios of 100, 200, 300 and 500 were labeled as SZ11-1, SZ11-2, SZ11-3 and SZ11-4, respectively. The zeolite content of ZSM-11/SS-fiber catalyst was estimated by the weight gain of the pristine microfibrous substrates after hydrothermal synthesis. For comparison, the synthesis precursor for the preparation of SZ11-2 was directly hydrothermally treated under the same conditions as the ZSM-11/SS-fiber catalysts to get powder ZSM-11 catalyst.

2.2. Catalyst characterization

Powder X-ray diffraction (XRD) patterns were collected on a Rigaku Ultima IV desktop X-ray diffractometer with monochromated Cu Kα radiation (0.154 nm, 35 kV, and 25 mA). N_2 adsorption/desorption isotherms were measured at 77 K on a Quantachrome Autosorb-iQ3 gas adsorption analyzer. For the sole ZSM-11 coated on SS-fiber, specific surface area (SSA) and pore volume were calculated via dividing the as-measured data of the ZSM-11/SS-fiber catalyst by the zeolite mass content. The actual SiO_2/Al_2O_3 molar ratio of ZSM-11/SS-fiber catalyst was determined by inductively coupled plasma atomic emission spectroscopy (ICP-AES, ICP Thermo IRIS Intrepid II XSP, USA). The surface morphology of ZSM-11/SS-fiber catalyst was characterized by the scanning electron microscopy (SEM, Zeiss Ultra, Germany). Temperature-programmed desorption of ammonia (NH_3-TPD) was performed on a Quantachrome ChemBET Pulsar chemisorption analyzer.

2.3. Catalyst performance test

The obtained microfibrous-structured ZSM-11/SS-fiber catalysts were tested in the dehydration of glycerol. A continuous-flow fixed-bed quartz tube reactor (i.d. of 8 mm; reactor length of 650 mm) was used for such reaction at 290-320 ºC and glycerol weight hourly space velocity (WHSV, represents the mass of glycerol per gram of ZSM-11, per hour) of 0.75 h^{-1}

under atmospheric pressure. Circular chips (8 mm diameter) of the ZSM-11/SS-fiber catalysts were packed layer-by-layer into the tube reactor. The zeolite mass in the microfibrous-structured catalysts was 0.1 g (not including the mass of SS-fiber). Prior to the catalytic tests, catalyst bed was pretreated at 300 ºC for 1 h in flowing N_2 (30 mL min^{-1}). A preheater was located on top of the reactor to vaporize the feed (vaporization temperature 260 ºC). By using a high-performance liquid chromatography (HPLC) pump, 10-20 wt.% glycerol solution in water was fed continuously and nitrogen was used as the carrier gas (10-50 mL min^{-1}). The products and unconverted reactant after different time-on-stream (TOS) values were collected in a vial cooled with an ice trap. The collected liquid was analyzed using a Shimadzu GC-2014 gas chromatograph equipped with a flame ionization detector and a capillary column (Rtx-WAX, 30 m, 0.25 mm, 0.25 μm). Glycerol conversion was calculated on the basis of mol of glycerol at the inlet and outlet of the reactor. Product selectivity was defined as the molar ratio of carbon in the products formed versus the glycerol converted.

3. RESULTS AND DISCUSSION

3.1. Geometry, morphology and structural features of ZSM-11/SS-fiber

Figure 1a shows the SEM image of pristine SS-fiber substrate, in which ~20 μm metal fibers were sinter-locked with each other, delivering a superior heat transfer performance and 3D open macroporous structure. Figures 1b-f show the geometry, morphology, and structural/textural properties of our representative catalyst prepared using a synthesis precursor with SiO_2/Al_2O_3 molar ratio of 200, denoted as SZ11-2. In comparison with the pristine SS-microfibrous structure (Figure 1a), by in-situ hydrothermal synthesis in a mixed solution of silica sol, $NaAlO_2$ and TBAOH, a uniform and dense zeolite layer was formed continuously along with the SS-fiber to form 3D-network ZSM-11/SS-fiber monolithic structure while macropores of the sinter-locked

structure are well-preserved (Figures 1b-d). The SEM image in Figure 1d shows that the zeolite layer consists of abundant well-crystallized particles with a size of ~300 nm. Notably, a high ZSM-11 zeolite loading of ~17.3 wt.% was achieved after only two synthesis cycles (seeding and hydrothermal treatment) with a zeolite layer thickness of ~4.5 μm (Figure 1d). Due to the intergrowth of crystals and core (SS-fiber)@shell (ZSM-11) structure, this microstructured ZSM-11/SS-fiber composite has a good adherence of zeolite layer, showing negligible weight loss after ultrasonic treatment in ethanol for 20 h. The XRD patterns in Figure 1e show that as-synthesized ZSM-11/SS-fiber composite exhibits typical MEL structure with high crystallinity, as evidenced by the major XRD diffraction peaks located at the ranges of 2θ = 7-9°, 2θ = 22-25° and single peak at ~45°, and no impurities phase was detected. The N_2 adsorption-desorption isotherms of the ZSM-11/SS-fiber in Figure 1f display a steep increase at very low relative pressure ($P/P_0 < 0.1$), indicating the well-constructed microporosity of ZSM-11 layer. Microstructured SZ11-2 catalyst with ~17.3 wt.% ZSM-11 zeolite presents a total BET specific surface area (SSA) of 69.8 $m^2\ g^{-1}$ with a micropore volume of 0.029 $cm^3\ g^{-1}$ (including the mass of SS-fiber).

Figure 2 shows the N_2 adsorption-desorption isotherms of the pure ZSM-11 layers in ZSM-11/SS-fiber catalysts with different SiO_2/Al_2O_3 molar ratios. All the four samples display a steep increase at very low relative pressure ($P/P_0 < 0.1$), indicating the well-constructed microporosity of ZSM-11 layer. The textural properties of pure ZSM-11 layer in different catalysts are listed in Table 1. The four samples possess a micropore SSA and volume of 324-372 $m^2\ g_{zeolite}^{-1}$ and 0.14-0.16 $cm^3\ g_{zeolite}^{-1}$ respectively (Table 1), comparable to the literature data [37-39]. In addition, small hysteresis loops can be seen at the relative pressure of 0.4-1.0 on isotherms, suggesting the ZSM-11/SS-fiber composites have appreciable mesopores in their zeolite layers. Figure S1 shows that

the size of these mesopores was distributed at <5 nm. For the sole zeolite layer in all the four catalysts, the mesopore volume is about 0.03-0.05 $cm^3\ g_{zeolite}^{-1}$ (Table 1).

SEM images in Figure 1c and Figure 3 show that the SZ11-1 catalyst with actual SiO_2/Al_2O_3 molar ratio of 78 (Table 1) featured with ~500 nm sized spherical crystallites, while the zeolite crystallites become larger and angular with the increase in the SiO_2/Al_2O_3 ratio up to 283. As previously noted [40-41], the apparent activation energies for pentasil zeolite (MFI and MEL types) nucleation as well as crystal growth are much lower in the aluminum-free cases than in the aluminum-containing system. Thus, ZSM-11 growth is favorable to form large crystals in case using a synthesis precursor with high SiO_2/Al_2O_3 molar ratios.

To identify the acidic properties of microstructured ZSM-11/SS-fiber catalysts with different SiO_2/Al_2O_3 molar ratios were characterized by means of NH_3-TPD. Figure 4 shows that the NH_3 desorption peaks centered at lower temperatures has an unchanged position of 260 ºC, while desorption peaks located at higher temperatures (420-450 ºC) associated with strong acid sites show downward trend as SiO_2/Al_2O_3 molar ratio increases. Meanwhile, it can also be observed that the area of desorption peaks for both weak and strong acid sites was decreased with the increase of SiO_2/Al_2O_3 molar ratio. Hence, the calculated results in Table 1 show that the SZ11-1 catalyst possessed the highest acid amounts of 324 μmol $g_{zeolite}^{-1}$, while lowest acid amount of 99 μmol $g_{zeolite}^{-1}$ was achieved on SZ11-4.

This series of microstructured ZSM-11 catalysts with various acidity by their SiO_2/Al_2O_3 molar ratios were tested in the dehydration of glycerol, at atmospheric pressure and 300 ºC, feeding to the catalytic bed with a WHSV of glycerol of 0.75 h^{-1}. The main products were acrolein, acetaldehyde, propanal and acetol. All the high molecular weight products with longer retention time in GC analysis were defined as “others”, including cyclic unsaturated and

oxygenated compounds formed by the secondary reaction of acrolein, as well as polyglycerols formed directly from the glycerol. The catalytic performance of ZSM-11/SS-fiber catalysts was gathered in Table 2. The initial glycerol conversion after 2 h on stream for all the four catalysts achieved a higher value, as the same as the previous publications [20, 23-24]. Especially, on SZ11-2 and SZ11-3, glycerol conversion was up to >90%. It is generally acknowledged that the catalytic activity for the dehydration of glycerol over zeolite catalysts was depended on the amounts of acid sites [18-19, 42]. Accordingly, microstructured ZSM-11 catalyst with lowest SiO_2/Al_2O_3 molar ratio should exhibit the best activity. However, glycerol conversion over SZ11-2 and SZ11-1 catalysts were much lower than SZ11-3. Kim et al. [20] found that increasing aluminum content made ZSM-5 more hydrophilic and strong adsorption of water molecules can also block the acid sites from being accessible for reactants. Since the composition and structure of ZSM-11 is quite similar to ZSM-5, the increased hydrophobicity should be the main reason for the decreased activity of SZ11-2 and SZ11-1 catalysts. A remarkable difference in acrolein selectivity and yield is also observed. The SZ11-2 catalyst shows the highest acrolein selectivity of 60.3% and yield of 57.7%. Microstructured catalysts with higher or lower SiO_2/Al_2O_3 molar ratios were all adverse to the formation of acrolein. Moreover, the SZ11-2 catalyst achieved the best stability, delivering a glycerol conversion of 44.6% after 5 h on stream.

3.2.2. Effect of the reaction temperature

Table 3 summarizes the results of the reaction temperature dependence of the glycerol dehydration reaction over SZ11-2 catalyst. The glycerol conversion over SZ11-2 catalyst at 290 ^oC was relatively lower after 2 h on stream, so higher temperature of ≥300 ^oC was necessary to achieve better catalytic performance. Such observation was in good agreement with the results on ZSM-5 [20], β [18], ferrierite [18] and MCM-22 [19]. However, one previous literature [4] reported that

increasing reaction temperature can cause a partial shift toward the production of acetol and acid, due to the higher extent of secondary reactions resulting from the higher temperature and more glycerol and intermediates trapped on the catalyst. It was not observed in microstructured ZSM-11/SS-fiber catalysts in this research. For microstructured ZSM-11/SS-fiber, higher reaction temperatures were also adverse to the formation of target product acrolein. As shown in Table 3, the acrolein selectivity decreased from 60.3% to 47.2% with yield from 57.7% to 44.1% as the temperature was increased from 300 ºC to 320 ºC. Meanwhile, the acetaldehyde selectivity showed a monotonous increase with the temperature increasing, because the formation of acetaldehyde was mainly due to the thermal decomposition of acrolein [19]. After reaction for 5 h, SZ11-2 catalyst tested at higher temperature showed less activity degeneration than that at lower temperatures. For example, a highest conversion of 49.0% was achieved at 320 ºC, while it has decreased to 22.9% at 290 ºC. On the contrary, high temperature caused a lowest acrolein selectivity, and most of the converted glycerol molecules were transformed into high molecular weight products.

3.2.3. Effect of carrier gas flow rate and glycerol content

The variation in carrier gas flow rate and glycerol content over SZ11-2 catalyst was shown in Table 4. As long as the N_2 flow rate was in the range from 10 mL min^{-1} to 50 mL min^{-1}, there was no noticeable difference in the glycerol conversion after 2 h on stream. However, a significant decrease of acrolein selectivity from 68.1% to 38.0% was observed, while the selectivity towards high molecular weight products was greatly increased from 25.9% to 54.0%. Generally, the increased carrier gas flow rate was associated with a decreased contact time between reactant/products molecules and acid sites, which would tend to retard the multimolecular reactions or side reactions. However, catalytic results showed that higher carrier

gas flow rate impeded the formation of acrolein but favored for the formation of high molecular weight products. Hence, it is possible to conclude that parts of the compounds grouped in "others" are formed directly from the glycerol, such as oligomers (polyglycerols) [43], being primary products, which may more easily form under shorter contact time. On the other hand, the increased selectivity of high molecular weight products made no influence on the SZ11-2 catalyst. After reaction for 5 h, the glycerol conversion has decreased to 30.3% under 10 mL min^{-1} N_2 flow, but it was still higher than 40% under N_2 flow of 30 50 mL min^{-1} and 50 mL min^{-1}. Such observation indicated that coke formation was suppressed due to the enhanced diffusion of high molecular weight products by high-flow carrier gas. In comparison with carrier gas flow rate, glycerol content in water solution has more intensive effects on the reaction performance. The SZ11-2 catalyst tested under 30 mL min^{-1} N_2 flow and 20 wt.% glycerol feeding showed both lower activity and acrolein selectivity. Kim et al. [20] reported that the presence of water vapor on the surface of zeolite catalyst can modulate the subsequent reaction of the chemisorbed glycerol and promote the selective formation toward acrolein because glycerol is chemisorbed on the acid sites predominantly over water vapor. So, decreasing the concentration of water vapor can facilitate side reactions such as bimolecular condensation reactions to form larger molecules. Over SZ11-2 catalyst, further reactions starting from acrolein are accelerated due to the decreased water vapor, thereby resulting a decrease in the acrolein selectivity with decreasing water content in the feed.

3.2.4. Insight into the microstructured design

To illuminate the importance of microstructured design more clearly, a powdered ZSM-11 catalyst was prepared by the same method as the SZ11-2 catalyst but without using SS-fiber substrate and was tested in the glycerol dehydration. As shown in Figure 5, the glycerol

conversion over such powdered ZSM-11 was obviously lower than the microstructured SZ11-2 catalyst over the whole test time. After 5 h reaction, glycerol conversion has decreased to below 20% for ZSM-11, less than half of that (44.6%) for microstructured SZ11-2 catalyst. Meanwhile, ZSM-11 also showed lower acrolein selectivity as compared to SZ11-2 catalyst. Due to the same synthesis precursor used for both powder ZSM-11 and SZ11-2, such two catalysts had very similar properties in morphology and acidity (Figures S2-S3). So, the catalytic performance improvement of SZ11-2 catalyst should be mainly ascribed to its microstructured design. Acrolein is highly reactive under glycerol dehydration reaction conditions, which will suffer from secondary reactions such as condensation and oligomerization to forming high molecular weight products [44-45]. These products are cyclic unsaturated and oxygenated compounds such as phenol, dihydrofuran, cyclopentenone, methyl cyclopentenone and cyclohexenone, which are responsible for coke formation and cause the catalyst deactivation. Since the narrower residence time distribution and higher diffusion efficiency originated from microfibrous structure can inhibit the secondary reactions in consecutive reaction [46], microstructured SZ11-2 delivered both higher stability and selectivity than conventional powdered ZSM-11 catalyst.

4. CONCLUSIONS

The microstructured ZSM-11/SS-fiber catalyst was prepared by in-situ hydrothermal growth of zeolite layer on the SS-fiber support. The acid properties of obtained ZSM-11/SS-fiber catalysts were controllable via tuning the SiO_2/Al_2O_3 ratios in a wide range from 78 to 283. Therefore, the density of surface bridging SiOHAl groups acted as Brønsted acid sites can be tuned to optimize the catalytic performance, since the Brønsted acid sites are easier to access the center hydroxyl of glycerol for starting the dehydration towards acrolein. The highest glycerol conversions and acrolein selectivity were observed over the catalyst with a SiO_2/Al_2O_3 molar ratio of 131. The

higher temperature at 300 °C was necessary to achieve better catalytic conversion and improve the formation of target product acrolein. Further increasing temperature higher than 320 °C, the thermal decomposition of acrolein occurs to form the acetaldehyde, then followed by the coke formation. The coke formation was suppressed due to the enhanced diffusion of high molecular weight products by the high-flow carrier gas. In addition, glycerol content in water solution has intensive effects on the reaction performance. The optimized ZSM-11/SS-fiber catalyst delivered remarkable stability improvement as compared to the powdered ZSM-11 catalyst, because of its narrower residence time distribution and higher diffusion efficiency by the microfibrous-structured design, which suppressed the secondary reactions in the dehydration of glycerol to acrolein.

ASSOCIATED CONTENT

Supporting Information. Additional characterization results of microstructured ZSM-11/SS-fiber and powdered ZSM-11 catalysts, including Barrett-Joyner-Halenda (BJH) mesopore size distribution, SEM image and NH_3-TPD profile.

AUTHOR INFORMATION

Corresponding Authors

* E-mail: ylu@chem.ecnu.edu.cn

* E-mail: jun.huang@sydney.edu.au

ORCID

Jia Ding: 0000-0003-0563-7273

Yong Lu: 0000-0002-5126-1476

Jun Huang: 0000-0001-8704-605X

ACKNOWLEDGMENT

We acknowledge the financial supports from Australian Research Council Discovery Projects (DP150103842, DP180104010) the SOAR Fellowship, the Sydney Nano Grand Challenge from the University of Sydney, the National Natural Science Foundation of China (21773069, 21703069, 21473057, U1462129) and the Basic Key Project (18JC1412100) from the Shanghai Municipal Science and Technology Commission.

REFERENCES

1. Talebian-Kiakalaieh, A.; Amin, N. A. S.; Hezaveh, H., Glycerol for renewable acrolein production by catalytic dehydration. *Renew. Sus. Energy Rev.* **2014,** *40*, 28-59.
2. Dodekatos, G.; Schünemann, S.; Tüysüz, H., Recent advances in thermo-, photo-, and electrocatalytic glycerol oxidation. *ACS Catal.* **2018,** *8* (7), 6301-6333.
3. Katryniok, B.; Paul, S.; Bellière-Baca, V.; Rey, P.; Dumeignil, F., Glycerol dehydration to acrolein in the context of new uses of glycerol. *Green Chem.* **2010,** *12* (12), 2079-2098.
4. Corma, A.; Huber, G.; Sauvanaud, L.; Oconnor, P., Biomass to chemicals: Catalytic conversion of glycerol/water mixtures into acrolein, reaction network. *J. Catal.* **2008,** *257* (1), 163-171.
5. Schuh, K.; Kleist, W.; Høj, M.; Trouillet, V.; Beato, P.; Jensen, A. D.; Patzke, G. R.; Grunwaldt, J.-D., Selective oxidation of propylene to acrolein by hydrothermally synthesized bismuth molybdates. *Appl. Catal. A* **2014,** *482*, 145-156.

6. Zhao, C.; Wachs, I. E., Selective oxidation of propylene to acrolein over supported V_2O_5/Nb_2O_5 catalysts: An in situ Raman, IR, TPSR and kinetic study. *Catal. Today* **2006,** *118* (3), 332-343.

7. Mahdavi, V.; Monajemi, A., Gas phase dehydration of glycerol catalyzed by gamma Al_2O_3 supported V_2O_5: A statistical approach for simultaneous optimization. *RSC Adv.* **2016,** *6* (115), 114244-114255.

8. Cecilia, J. A.; García-Sancho, C.; Mérida-Robles, J. M.; Santamaría González, J.; Moreno-Tost, R.; Maireles-Torres, P., WO_3 supported on Zr doped mesoporous SBA-15 silica for glycerol dehydration to acrolein. *Appl. Catal. A* **2016,** *516*, 30-40.

9. Chai, S.-H.; Yan, B.; Tao, L.-Z.; Liang, Y.; Xu, B.-Q., Sustainable production of acrolein: Catalytic gas-phase dehydration of glycerol over dispersed tungsten oxides on alumina, zirconia and silica. *Catal. Today* **2014,** *234*, 215-222.

10. García-Sancho, C.; Cecilia, J. A.; Moreno-Ruiz, A.; Mérida-Robles, J. M.; Santamaría-González, J.; Moreno-Tost, R.; Maireles-Torres, P., Influence of the niobium supported species on the catalytic dehydration of glycerol to acrolein. *Appl. Catal. B* **2015,** *179*, 139-149.

11. Xie, Q.; Li, S.; Gong, R.; Zheng, G.; Wang, Y.; Xu, P.; Duan, Y.; Yu, S.; Lu, M.; Ji, W.; Nie, Y.; Ji, J., Microwave-assisted catalytic dehydration of glycerol for sustainable production of acrolein over a microwave absorbing catalyst. *Appl. Catal. B* **2019,** *243*, 455-462.

12. Lauriol-Garbey, P.; Millet, J. M. M.; Loridant, S.; Bellière-Baca, V.; Rey, P., New efficient and long-life catalyst for gas-phase glycerol dehydration to acrolein. *J. Catal.* **2011,** *281* (2), 362-370.

13. Ren, X.; Zhang, F.; Sudhakar, M.; Wang, N.; Dai, J.; Liu, L., Gas-phase dehydration of glycerol to acrolein catalyzed by hybrid acid sites derived from transition metal hydrogen phosphate and meso-HZSM-5. *Catal. Today* **2018**.
14. Cavani, F.; Guidetti, S.; Marinelli, L.; Piccinini, M.; Ghedini, E.; Signoretto, M., The control of selectivity in gas-phase glycerol dehydration to acrolein catalysed by sulfated zirconia. *Appl. Catal. B* **2010,** *100* (1-2), 197-204.
15. Choi, Y.; Park, H.; Yun, Y. S.; Yi, J., Effects of catalyst pore structure and acid properties on the dehydration of glycerol. *ChemSusChem* **2015,** *8* (6), 974-9.
16. Ma, T.; Ding, J.; Shao, R.; Xu, W.; Yun, Z., Dehydration of glycerol to acrolein over Wells–Dawson and Keggin type phosphotungstic acids supported on MCM-41 catalysts. *Chem. Eng. J.* **2017,** *316*, 797-806.
17. de Oliveira, A. S.; Vasconcelos, S. J. S.; de Sousa, J. R.; de Sousa, F. F.; Filho, J. M.; Oliveira, A. C., Catalytic conversion of glycerol to acrolein over modified molecular sieves: Activity and deactivation studies. *Chem. Eng. J.* **2011,** *168* (2), 765-774.
18. Kim, Y. T.; Jung, K.-D.; Park, E. D., A comparative study for gas-phase dehydration of glycerol over H-zeolites. *Appl. Catal. A* **2011,** *393* (1-2), 275-287.
19. Carriço, C. S.; Cruz, F. T.; Santos, M. B.; Pastore, H. O.; Andrade, H. M. C.; Mascarenhas, A. J. S., Efficiency of zeolite MCM-22 with different SiO_2/Al_2O_3 molar ratios in gas phase glycerol dehydration to acrolein. *Micropor. Mesopor. Mater.* **2013,** *181*, 74-82.
20. Kim, Y. T.; Jung, K.-D.; Park, E. D., Gas-phase dehydration of glycerol over ZSM-5 catalysts. *Micropor. Mesopor. Mater.* **2010,** *131* (1-3), 28-36.

21. Carriço, C. S.; Cruz, F. T.; dos Santos, M. B.; Oliveira, D. S.; Pastore, H. O.; Andrade, H. M. C.; Mascarenhas, A. J. S., MWW-type catalysts for gas phase glycerol dehydration to acrolein. *J. Catal.* **2016,** *334*, 34-41.

22. Jia, C.-J.; Liu, Y.; Schmidt, W.; Lu, A.-H.; Schüth, F., Small-sized HZSM-5 zeolite as highly active catalyst for gas phase dehydration of glycerol to acrolein. *J. Catal.* **2010,** *269* (1), 71-79.

23. Gu, Y.; Cui, N.; Yu, Q.; Li, C.; Cui, Q., Study on the influence of channel structure properties in the dehydration of glycerol to acrolein over H-zeolite catalysts. *Appl. Catal. A* **2012,** *429-430*, 9-16.

24. Lago, C. D.; Decolatti, H. P.; Tonutti, L. G.; Dalla Costa, B. O.; Querini, C. A., Gas phase glycerol dehydration over H-ZSM-5 zeolite modified by alkaline treatment with Na_2CO_3. *J. Catal.* **2018,** *366*, 16-27.

25. Wang, Z.; Wang, L.; Jiang, Y.; Hunger, M.; Huang, J., Cooperativity of Brønsted and Lewis Acid Sites on Zeolite for Glycerol Dehydration. *ACS Catal.* **2014,** *4* (4), 1144-1147.

26. Possato, L. G.; Chaves, T. F.; Cassinelli, W. H.; Pulcinelli, S. H.; Santilli, C. V.; Martins, L., The multiple benefits of glycerol conversion to acrolein and acrylic acid catalyzed by vanadium oxides supported on micro-mesoporous MFI zeolites. *Catal. Today* **2017,** *289*, 20-28.

27. Beerthuis, R.; Huang, L.; Shiju, N. R.; Rothenberg, G.; Shen, W.; Xu, H., Facile Synthesis of a Novel Hierarchical ZSM-5 Zeolite: A Stable Acid Catalyst for Dehydrating Glycerol to Acrolein. *ChemCatChem* **2018,** *10* (1), 211-221.

28. Vieira, L. H.; Carvalho, K. T. G.; Urquieta-González, E. A.; Pulcinelli, S. H.; Santilli, C. V.; Martins, L., Effects of crystal size, acidity, and synthesis procedure on the catalytic

performance of gallium and aluminum MFI zeolites in glycerol dehydration. *J. Mol. Catal. A* **2016,** *422*, 148-157.

29. Possato, L. G.; Diniz, R. N.; Garetto, T.; Pulcinelli, S. H.; Santilli, C. V.; Martins, L., A comparative study of glycerol dehydration catalyzed by micro/mesoporous MFI zeolites. *J. Catal.* **2013,** *300*, 102-112.
30. Zhang, H.; Hu, Z.; Huang, L.; Zhang, H.; Song, K.; Wang, L.; Shi, Z.; Ma, J.; Zhuang, Y.; Shen, W.; Zhang, Y.; Xu, H.; Tang, Y., Dehydration of Glycerol to Acrolein over Hierarchical ZSM-5 Zeolites: Effects of Mesoporosity and Acidity. *ACS Catal.* **2015,** *5* (4), 2548-2558.
31. Decolatti, H. P.; Dalla Costa, B. O.; Querini, C. A., Dehydration of glycerol to acrolein using H-ZSM5 zeolite modified by alkali treatment with NaOH. *Micropor. Mesopor. Mater.* **2015,** *204*, 180-189.
32. Maesen, T. L. M.; Schenk, M.; Vlugt, T. J. H.; Smit, B., Differences between MFI- and MEL-type zeolites in paraffin hydrocracking. *J. Catal.* **2001,** *203* (2), 281-291.
33. Ding, J.; Chen, P.; Zhao, G.; Liu, Y.; Lu, Y., High-performance thin-felt SS-fiber@HZSM-5 catalysts synthesized via seed-assisted vapor phase transport for methanol-to-propylene reaction: Effects of crystal size, mesoporosity and aluminum uniformity. *J. Catal.* **2018,** *360*, 40-50.
34. Ding, J.; Jia, Y.; Chen, P.; Zhao, G.; Liu, Y.; Lu, Y., Microfibrous-structured hollow-ZSM-5/SS-fiber catalyst with mesoporosity development dependent lifetime improvement for MTP reaction. *Micropor. Mesopor. Mater.* **2018,** *261*, 1-8.

35. Jiao, Y.; Yang, X.; Jiang, C.; Tian, C.; Yang, Z.; Zhang, J., Hierarchical ZSM-5/SiC nano-whisker/SiC foam composites: Preparation and application in MTP reactions. *J. Catal.* **2015,** *332*, 70-76.

36. Jiao, Y.; Ou, X.; Zhang, J.; Fan, X., Structured ZSM-5 coated SiC foam catalysts for process intensification in catalytic cracking of n-hexane. *React. Chem. Eng.* **2019,** *4* (2), 427-435.

37. Yu, Q.; Tang, X.; Yi, H., The role of Al species on the formation of hierarchical morphology of ZSM-11 zeolite. *Mater. Chem. Phys.* **2017,** *202*, 377-384.

38. Zhang, L.; Liu, H.; Li, X.; Xie, S.; Wang, Y.; Xin, W.; Liu, S.; Xu, L., Differences between ZSM-5 and ZSM-11 zeolite catalysts in 1-hexene aromatization and isomerization. *Fuel Process. Technol.* **2010,** *91* (5), 449-455.

39. Wei, Z.; Zhu, K.; Xing, L.; Yang, F.; Li, Y.; Xu, Y.; Zhu, X., Steam-assisted transformation of natural kaolin to hierarchical ZSM-11 using tetrabutylphosphonium hydroxide as structure-directing agent: synthesis, structural characterization and catalytic performance in the methanol-to-aromatics reaction. *RSC Adv.* **2017,** *7* (39), 24015-24021.

40. Erdem, A.; Sand, L. B., Crystallization and metastable phase transformations of zeolite ZSM-5 in the $(TPA)_2O$-Na_2O-K_2O-Al_2O_3-SiO_2-H_2O system. *J. Catal.* **1979,** *60* (2), 241-256.

41. Yu, Q.; Tang, X.; Yi, H., Fabrication of ZSM-11(5) particles with nanorods oriented-stacking morphology by an in-situ feeding method. *Chem. Eng. J.* **2017,** *314*, 212-222.

42. Suprun, W.; Lutecki, M.; Haber, T.; Papp, H., Acidic catalysts for the dehydration of glycerol: Activity and deactivation. *J. Mol. Catal. A* **2009,** *309* (1-2), 71-78.

43. Barrault, J.; Clacens, J. M.; Pouilloux, Y., Selective Oligomerization of Glycerol Over Mesoporous Catalysts. *Top. Catal.* **2004,** *27* (1), 137-142.

44. Witsuthammakul, A.; Sooknoi, T., Direct conversion of glycerol to acrylic acid via integrated dehydration-oxidation bed system. *Appl. Catal. A* **2012,** *413-414*, 109-116.

45. Chai, S.-H.; Wang, H.-P.; Liang, Y.; Xu, B.-Q., Sustainable production of acrolein: Investigation of solid acid–base catalysts for gas-phase dehydration of glycerol. *Green Chem.* **2007,** *9* (10), 1130-1136.

46. Wen, M.; Ding, J.; Wang, C.; Li, Y.; Zhao, G.; Liu, Y.; Lu, Y., High-performance SS-fiber@HZSM-5 core-shell catalyst for methanol-to-propylene: A kinetic and modeling study. *Micropor. Mesopor. Mater.* **2016,** *221*, 187-196.

Table 1 Textural and acidic properties of the zeolite layer in the microstructured ZSM-11/SS-fiber with various SiO_2/Al_2O_3 molar ratios.

Sample	SiO_2/Al_2O_3[a]	S_{BET}[b] ($m^2 g_{zeolite}^{-1}$)	S_{micro}[c] ($m^2 g_{zeolite}^{-1}$)	V_{micro}[d] ($cm^3 g_{zeolite}^{-1}$)	V_{meso}[e] ($cm^3 g_{zeolite}^{-1}$)	V_{total}[f] ($cm^3 g_{zeolite}^{-1}$)	Acidity[g] (μmol $g_{zeolite}^{-1}$)		
							Strong	Weak	Total
SZ11-1	78	378	324	0.14	0.05	0.19	149	175	324
SZ11-2	131	403	372	0.16	0.03	0.19	97	99	196
SZ11-3	203	400	360	0.16	0.04	0.20	65	65	130
SZ11-4	283	365	326	0.15	0.03	0.18	47	52	99

[a] SiO_2/Al_2O_3 molar ratios determined by ICP-AES. [b] BET specific surface area determined by Brunauer-Emmett-Teller method. [c] Micropore specific surface area. [d] Micropore volume determined by the t-plot method. [e] Mesopore volume. [f] Total pore volume at $p/p_0 = 0.95$. [g] The quantities of weak and strong acid sites determined by NH_3-TPD.

Table 2 Glycerol conversion and products selectivity over different SZ11-x catalysts.

Sample	SZ11-1		SZ11-2		SZ11-3		SZ11-4	
TOS	2 h	5 h	2 h	5 h	2 h	5 h	2 h	5 h
Glycerol conv. (%)	70.1	13.9	95.7	44.6	90.0	42.2	79.3	30.4
Acrolein yield (%)	20.1	5.7	57.7	21.4	45.0	20.1	20.2	5.2
Selectivity (%)								
Acetaldehyde	2.1	2.9	5.2	3.8	4.5	4.1	2.6	1.7
Propanal	0.8	1.1	1.1	1.3	0.9	1.4	2.2	3.1
Acetol	4.9	13.5	0.8	6.7	2.4	9.1	10.4	16.8
Acrolein	28.6	40.8	60.3	47.9	50.0	47.8	25.5	17.0
Others	63.6	41.7	32.6	40.3	42.2	37.6	59.3	61.4

Table 3 Glycerol conversion and products selectivity over SZ11-2 catalyst at different temperatures.

Temperature (°C)	290		300		310		320	
TOS	2 h	5 h	2 h	5 h	2 h	5 h	2 h	5 h
Glycerol conv. (%)	84.9	22.9	95.7	44.6	95.3	46.3	93.5	49.0
Acrolein yield (%)	44.0	10.6	57.7	21.4	47.3	14.7	44.1	11.1
Selectivity (%)								
Acetaldehyde	3.7	3.2	5.2	3.8	7.1	3.8	13.1	3.4
Propanal	1.0	1.9	1.1	1.3	1.3	2.6	2.5	2.7
Acetol	1.1	5.3	0.8	6.7	1.6	6.5	2.0	7.5
Acrolein	51.8	46.3	60.3	47.9	49.6	31.8	47.2	22.7
Others	42.4	43.3	32.6	40.3	40.5	55.3	35.2	63.7

Table 4 Glycerol conversion and products selectivity over SZ11-2 catalyst at different glycerol contents and carrier gas flow rates.

Glycerol content (wt.%) and N_2 flow rate (mL min^{-1})	10 & 10		10 & 30		10 & 50		20 & 30	
TOS	2 h	5 h	2 h	5 h	2 h	5 h	2 h	5 h
Glycerol conv. (%)	92.2	30.3	95.7	44.6	93.5	43.0	80.2	29.6
Acrolein yield (%)	62.8	19.1	57.7	21.4	35.5	11.4	25.0	8.5
Selectivity (%)								
Acetaldehyde	3.4	3.6	5.2	3.8	3.4	2.4	2.9	3.0
Propanal	0.3	0.8	1.1	1.3	1.0	1.0	0.9	1.6
Acetol	2.3	5.7	0.8	6.7	3.6	13.7	2.8	10.2
Acrolein	68.1	63.0	60.3	47.9	38.0	26.5	31.2	28.7
Others	25.9	26.9	32.6	40.3	54.0	56.4	62.2	56.5

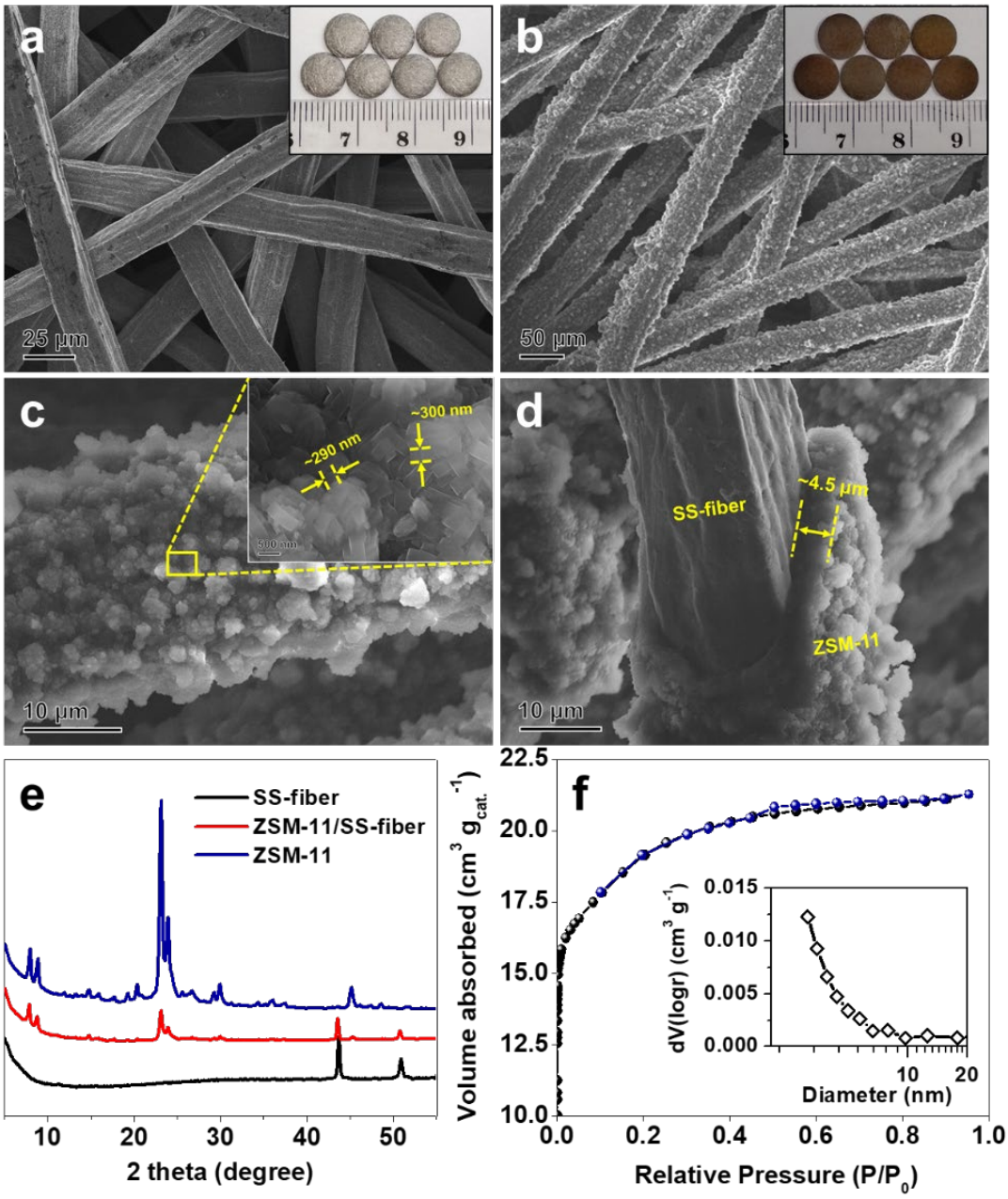

Figure 1. All in one figure for the representative ZSM-11/SS-fiber catalyst with SiO_2/Al_2O_3 molar ratio of 200 and zeolite content of ~17.3 wt.%. (a) Photograph and SEM image of the pristine SS-fiber substrate; (b-d) photograph and SEM images of ZSM-11/SS-fiber; (e) XRD patterns; (f) N_2 adsorption-desorption isotherms and Barrett-Joyner-Halenda (BJH) mesopore size distribution (inset).

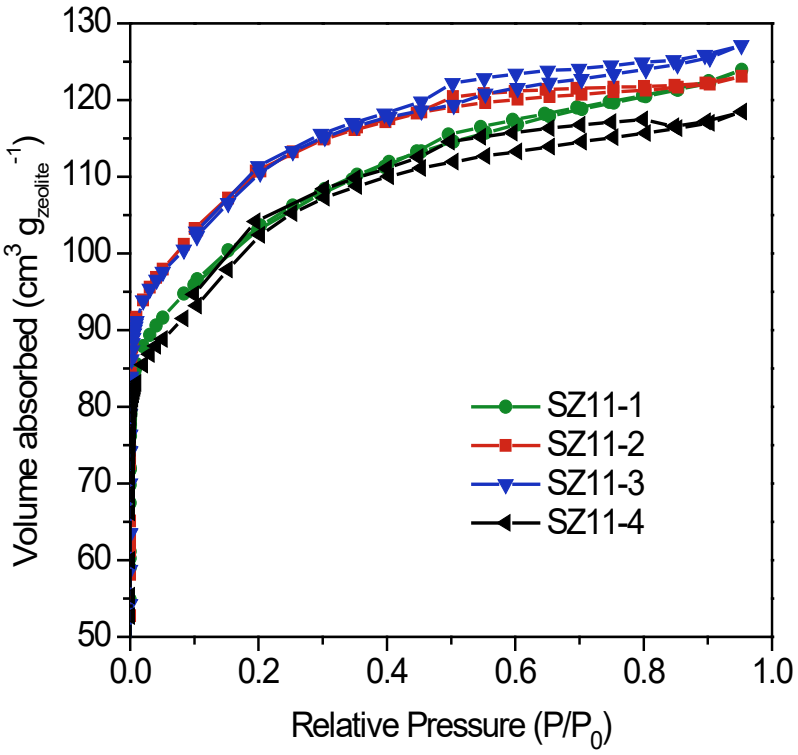

Figure 2. N_2 adsorption-desorption isotherms of the pure zeolite layers in ZSM-11/SS-fiber catalysts with various SiO_2/Al_2O_3 molar ratios (not including the mass of SS-fiber).

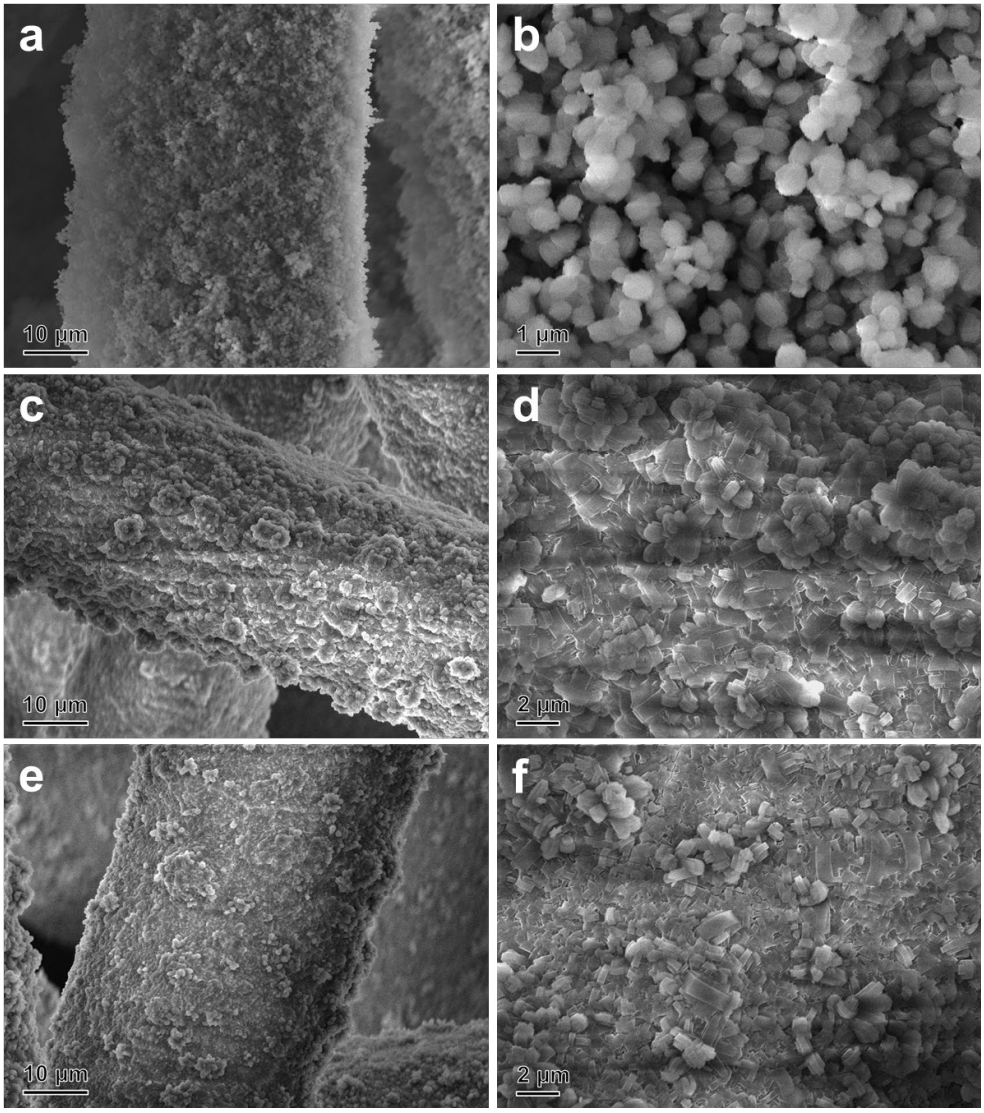

Figure 3. SEM images of (a,b) SZ11-1, (c,d) SZ11-3, and (e,f) SZ11-4 catalysts with various SiO_2/Al_2O_3 molar ratios.

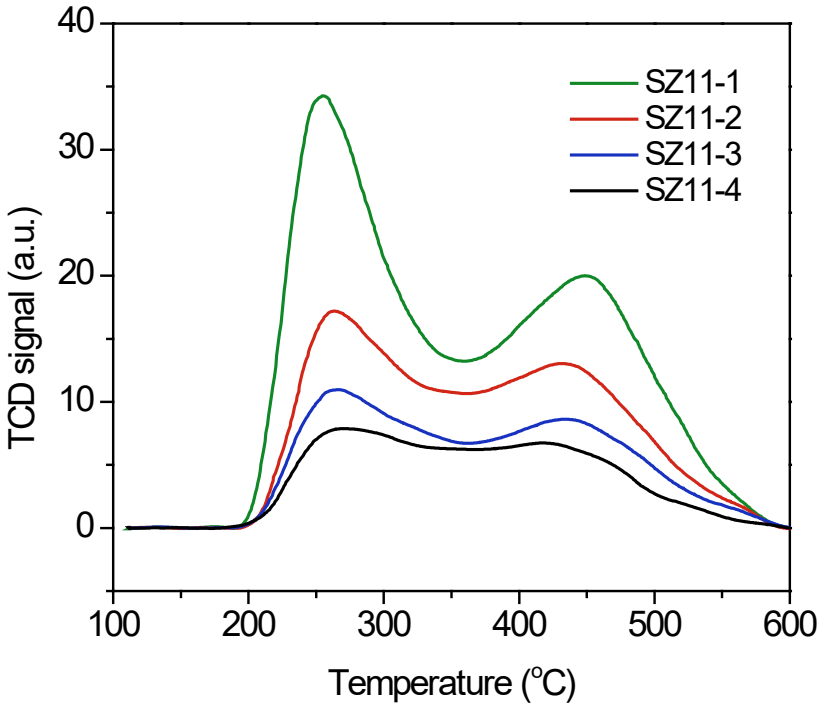

Figure 4. NH_3-TPD profiles of the ZSM-11/SS-fiber catalysts with various SiO_2/Al_2O_3 molar ratios.

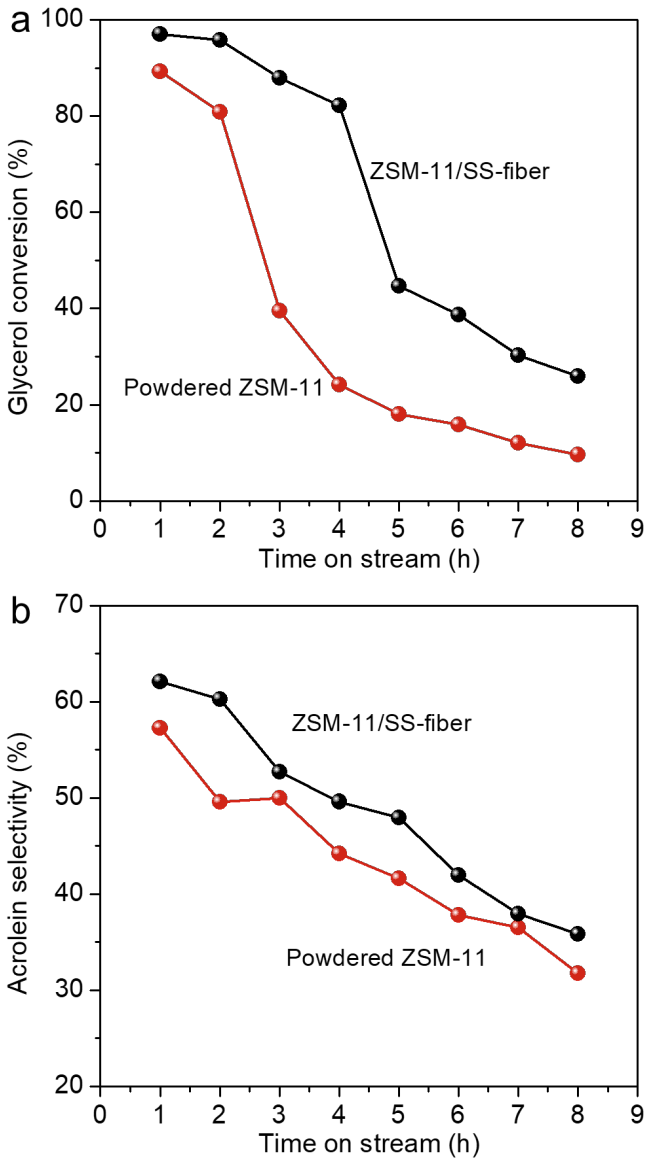

Figure 5. (a) Glycerol conversion and (b) acrolein selectivity against time on stream using the ZSM-11/SS-fiber and powdered ZSM-11 catalysts. Reaction conditions: 300 ºC, 10 wt.% glycerol in water, N_2 flow rate of 30 mL min^{-1}, zeolite mass of 0.4 g.

TABLE OF CONTENTS (TOC)

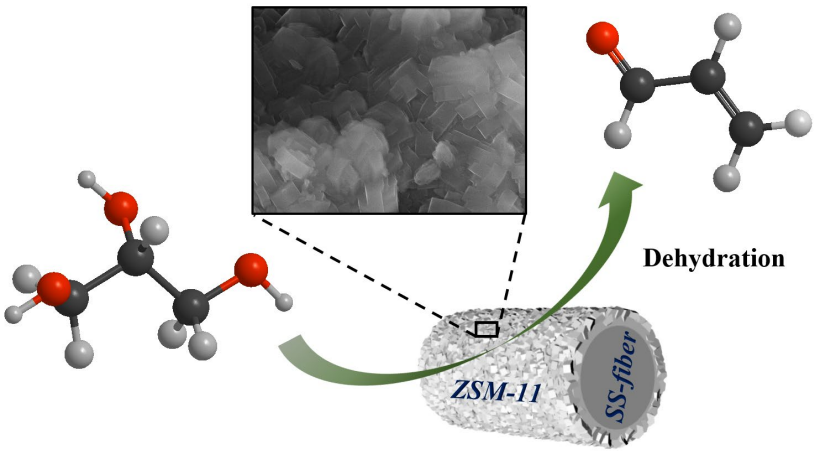

SYNOPSIS: Micro-structured ZSM-11 catalyst on stainless-steel (SS) microfibers was fabricated with improved catalytic performance in glycerol dehydration to acrolein.